



RESEARCH ARTICLE

The performance improvement of a cascade thermoacoustic engine by adjusting the acoustic impedance in the regenerator

Isares Dhuchakallaya^{1,*}, Patcharin Saechan² and Phadungsak Rattanadecho¹¹Department of Mechanical Engineering, Faculty of Engineering, Thammasat University, Klong-Luang, Pathumthani, 12120, Thailand²Department of Mechanical and Aerospace Engineering, Faculty of Engineering, King Mongkut's University of Technology North Bangkok, Bangsue, Bangkok, 10800, Thailand

SUMMARY

A novel cascade configuration consisting of one standing wave unit and one travelling wave unit arranged in series is studied in this paper. Theoretically, a straight-line cascade engine provides an efficient energy conversion, reduces the difficulties of fabrication and allows no Gedeon streaming. In order to achieve such a powerful cascade thermoacoustic engine, the regenerator of the travelling wave unit must be operated in high impedance and travelling wave phasing region. Various techniques of phase adjustment by modifying the configurations and geometrical dimensions of the system are investigated both numerically and experimentally in order to adjust the position of the sweet spot as well as to promote the acoustic impedance in the regenerator. It is found that the effective tuning methods with less modification here are accomplished by changing the volume of down-cavity and reducing the flow area of down-resonator by inserting the pencil. The exploration also shows that the acoustic field in the system is quite sensitive to the effect of down-resonator length. The performance of the proposed system is clearly improved after the phase-adjustment schemes are completely implemented, in which the regenerator works within the sweep spot zone with high acoustic impedance. Copyright © 2016 John Wiley & Sons, Ltd.

KEY WORDS

cascade; phase adjustment; sweet spot; thermoacoustic engine; travelling wave phasing

Correspondence

*Isares Dhuchakallaya, Department of Mechanical Engineering, Faculty of Engineering, Thammasat University, Klong-Luang, Pathumthani 12120, Thailand.

†E-mail: dhuchakallaya@yahoo.com

Received 10 May 2016; Revised 6 August 2016; Accepted 6 August 2016

1. INTRODUCTION

Thermoacoustic engines are concerned with the conversion between thermal and acoustic energies. The acoustic power generated by such devices can be employed to generate electricity through electro-dynamic transducers, or to drive thermoacoustic refrigeration. Typically, thermoacoustic engines can be classified into two types: 'standing-wave' and 'travelling-wave' engines, depending on whether the acoustic pressure and velocity are 90° out of phase or in phase, respectively. The phase difference of pressure and velocity has affected the heat transfer between the working gas and solid material in the thermoacoustic core. In the standing wave engine, imperfect thermal contact occurs because of the time delay between the thermal processes and the gas motion. However, it is not necessary in the travelling wave engine. Therefore, the gas temperature is always equal to the solid temperature. Hence, the

efficiency of thermo-to-acoustic conversion, defined as the ratio between the generated acoustic power from the engine and the heat input, of the travelling wave engines is higher than the standing wave engines [1].

Because of the high efficiency of the travelling wave thermoacoustic devices, the research related to such devices has been developed rapidly since they were demonstrated by Ceperley [2,3]. However, the efficiency was only 10% of Carnot efficiency. Yazaki *et al.* [4] proposed a looped-tube travelling wave thermoacoustic engine. Its efficiency was better than the Ceperley's engine. However, the problem of low acoustic impedance in a regenerator still exists. It was successfully fixed out with the new design of such engine by connecting a side branch resonator to a loop tube. This typical layout is called as thermoacoustic-Stirling engine [5], which can provide up to 41% of the Carnot efficiency. To accomplish high efficiency, high acoustic impedance and travelling wave

phasing in the regenerator were required. An undesired heat leak by transferring heat from the hot-side to the cold-side without contributing to the thermoacoustic effect referred as acoustic streaming was suppressed by introducing the appropriate jet pump and taper thermal buffer tube (TBT) into the system. However, these requirements also increase the complexity of design and construction.

Recently, a cascade thermoacoustic engine (CTE) was developed [6] to reduce the complexity of construction and also provide relatively high efficiency. It is a straight-line configuration comprising of one standing wave unit (SWU) and two travelling wave units (TWU) cascaded within the high impedance zone. The acoustic power originated from the SWU is amplified successively by the TWUs. So the acoustic field in the resonator is the combination of the standing wave and travelling wave modes. This significantly improves the acoustic impedance in the regenerators of TWUs that is the drawback of the looped-tube engine. Since the units of engine are continually added into the CTE, the efficiency of system exponentially increases in the early stage and then limits to a particular level. Practically, only three or four stages can be fitted in one pressure anti-node. The efficiency of this cascade engine was only 30% of the Carnot efficiency. The further improved engine is anticipated to provide efficiency up to 40% which is equal to the highest efficiency of thermoacoustic engine so far [6].

Since the first CTE was proposed, continuous efforts have been made. Luo *et al.* [7] and Ling *et al.* [8] demonstrated the numerical analysis of the CTE. The effect of imaginary dissipation load on the acoustic field was also investigated. Hu *et al.* [9,10] designed and built a miniature CTE. The diameter ratio of stages was analysed to obtain the efficient device. Such cascade engines discussed in [7–10] were designed to operate at high pressure of helium, and had the same configuration which consisted of one standing wave stage and one travelling wave stage in series.

Furthermore, Biwa *et al.* [11] also investigated the effect of impedance phase (φ_z) at the centre of heated stack/regenerator on the amplification of acoustic power. In case of TWU, the maximum amplification of acoustic power was detected at $\varphi_z \approx 40^\circ$ instead of $\varphi_z \approx 0^\circ$. This would be the contribution of viscous losses in the regenerator which increased with temperature. While the maximum gain amplified by the SWU was obtained at

$\varphi_z \approx 80^\circ$. This study is advantageous to the conception of cascade topology that the stack and regenerators are placed in series near the velocity node.

As reviewed above, the CTE is quite interesting because of its simplicity and relatively high efficiency. Most research in the particular field has only focused on achieving as high as possible energy conversion efficiency, often without any cost being a particular concern. Therefore, such systems were required to operate with a high pressure of valuable gases (e.g. argon, helium). One of the key challenges for improving the thermo-to-acoustic conversion of the CTE is to accurately configure and adjust the acoustic impedance because there is more than one stage coupled together and more uncertain boundary conditions. Because of under the combined mode of the standing wave and travelling wave in the system, the travelling wave zone might be insufficient to accommodate the regenerator. To obtain the efficient system, the high impedance and the travelling wave phasing are necessary located in the regenerator. Hence, the phase adjustment should be applied in order to fine-tune the acoustic impedance and phase difference between pressure and velocity in the regenerator. This leads to the research problem which is to investigate the effect of phase adjustment on the acoustic field.

2. CONCEPTUAL DESIGN AND NUMERICAL ANALYSIS

In this study, the CTE is designed to operate in one-wavelength mode with both end-cavities. Air at atmospheric pressure is used as working fluid because of its availability. This CTE is planned to drive the thermoacoustic refrigeration, so that the two-stage engine within a high impedance zone seems to be reasonable and less complicated to design and construct.

The configuration of system is conceptually designed as shown schematically in Figure 1. The system consists of one SWU and one TWU. The main components in each subsystem comprise of ambient heat exchanger (AHX), regenerator (REG) or stack (STK) and hot heat exchanger (HHX). In order to prevent heat leaks from the HHX of SWU to the AHX of TWU, the TBT is applied to separate them away. The AHX is used to maintain the cold end of REG or STK at ambient temperature. The REG and STK are made up from the mesh screens. The hydraulic radius

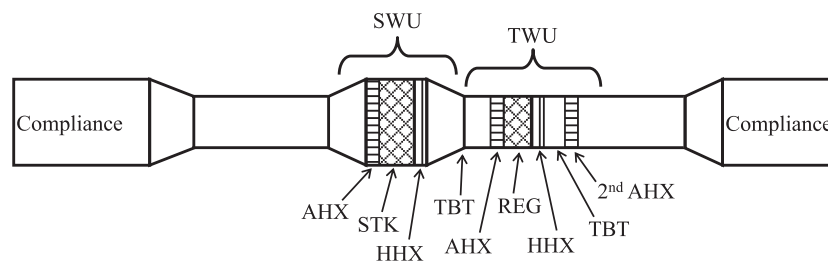


Figure 1. Schematic diagrams of the cascade thermoacoustic engine.

of mesh screen in the SWU is comparable to the thermal penetration depth ($\delta_k = \sqrt{k/\pi f \rho_m c_p}$), but is much smaller than δ_k in the TWU. Therefore, an excellent thermal contact between the working fluid and solid in the REG can be realised. The secondary ambient heat exchanger (2nd AHX) is added in order to eliminate the surplus heat of the hot working gas after leaving the HHX.

In the design, the TWU should be located at almost the centre of the system, near the velocity node, in which phase of the acoustic impedance (φ_z) changes from positive 90° to negative 90° or vice versa. φ_z by which pressure leading velocity at the regenerator becomes zero is called as 'sweet spot' [6]. Therefore, the TWU must be located within the sweet spot region where $\varphi_z \approx \pm 45^\circ$. This provides an effective thermo-to-acoustic conversion because the travelling wave phasing and the acoustic field with high impedance can be achieved. Therefore, the adjustments of the position and length of the sweet spot region are very important.

Under the complicated boundary conditions and coupling effects between stages, the computational design is introduced in order to tune the sweet spot region with high impedance in the REG. The numerical simulative model of the CTE is built by DeltaEC [12]. The numerical design based on linear thermoacoustic theory can be described by the continuity, momentum and energy equations [13]. The changes in pressure amplitude (p_1), velocity amplitude (U_1) and mean temperature (T_m) across a thermoacoustic segment can be determined as illustrated below:

$$\frac{dp_1}{dx} = -i\omega\rho_m A_{gas}(1-f_v)U_1 \quad (1)$$

$$\frac{dU_1}{dx} = -\frac{i\omega A_{gas}}{a^2\rho_m} \left[1 + \frac{(\gamma-1)f_k}{1+\varepsilon_s} \right] p_1 + \frac{\beta(f_k-f_v)}{(1-f_v)(1-\sigma)(1+\varepsilon_s)} \frac{dT_m}{dx} U_1 \quad (2)$$

$$\frac{dT_m}{dx} = \frac{\dot{H}_2 - \frac{1}{2}\text{Re} \left[p_1 \tilde{U}_1 \left(1 - \frac{T_m \beta (f_k - f_v)}{(1+\varepsilon_s)(1+\sigma)(1-f_v)} \right) \right]}{\frac{\rho_m c_p |U_1|^2}{2A_{gas}\omega(1-\sigma)|1-f_v|^2} \text{Im} \left(\tilde{f}_v + \frac{(f_k - f_v)(1+\varepsilon_s f_v / f_k)}{(1+\varepsilon_s)(1+\sigma)} \right) - (A_{gas}k + A_s k_s)} \quad (3)$$

where ω is the angular frequency, A_{gas} and A_s are area of gas flow and area of solid material, respectively, ρ_m , p_m , c_p , γ , a , k , β and σ are mean density, mean pressure, isobaric specific heat capacity, specific heat ratio, speed of sound, thermal conductivity, thermal expansion coefficient and Prandtl number of working fluid, respectively, ε_s is correction factor for finite solid heat capacity, i is the imaginary unit. Re, Im and superscript \sim are the real part, the imaginary part and the conjugate complex quantity, respectively, f_v and f_k are viscous and thermal functions depending on the geometry of individual component, and

subscripts '1' and '2' indicate the first and second order of a variable.

In addition, the acoustic power (\dot{E}_2) produced or dissipated in any segment can be estimated as:

$$\frac{d\dot{E}_2}{dx} = \frac{1}{2} \text{Re} \left[\tilde{U}_1 \frac{dp_1}{dx} + \tilde{p}_1 \frac{dU_1}{dx} \right] \quad (4)$$

The acoustic power produced by the stack in the SWU can be simplified as [13]:

$$\frac{d\dot{E}_2}{dx} = \frac{1}{2} |p_1|^2 \omega A \frac{\gamma-1}{\gamma p_m} \text{Im}[-f_k] \left(\frac{dT_m/dx}{\nabla T_{crit}} - 1 \right) \quad (5)$$

where

$$\nabla T_{cr} = \frac{|p_1|/\rho_m c_p}{|U_1|/A\omega} \quad (6)$$

is the critical temperature gradient.

It can be seen that the acoustic power generated depends on the temperature gradient across the stack (dT_m/dx). If the temperature gradient is high enough, the generated acoustic power can be observed.

In the TWU, the amplified acoustic power can be approximated from [13]

$$\dot{E}_2 = \dot{E}_{2,0} \left(\frac{T_H}{T_0} - 1 \right) - \frac{3\mu\Delta x}{2Ar_h^2} |U_1|^2 - \frac{\omega^2 Ar_h^2 \Delta x}{6kT_m} |p_1|^2 \quad (7)$$

where $\dot{E}_{2,0}$ is the acoustic power entering the ambient end of the regenerator at ambient temperature T_0 .

The performance of the cascade engine is defined as the ratio of the acoustic powers generated by both thermoacoustic cores to the sum of the heat powers supplied to the HHXs,

$$\eta = \frac{\dot{E}_{2,SWU} + \dot{E}_{2,TWU}}{\dot{Q}_{SWU} + \dot{Q}_{TWU}} \quad (8)$$

As seen in the Eq. (5), the acoustic power originated in the system is proportional to the square of pressure amplitude. Therefore, the acoustic power produced can be roughly represented by the pressure amplitude.

The set of these equations (cf. Eqs. (1–4)) is solved simultaneously to determine the change of working fluid properties along each segment of the thermoacoustic

device. The x coordinate is referred to as the distance along the system describing the distribution of components, starting from the closed-end of the up-cavity; $x = 0$.

3. EXPERIMENTAL APPARATUS

The prototype of the CTE with the measurement setup is displayed in Figure 2. The core components are located at the middle of the system. The AHXs in the system were designed as the cross-flow heat exchangers that were made from a round aluminium block. Gas passages were made in the form of small holes drilled parallel to its centreline, and the cooling water passages were drilled perpendicular to the bundle of small holes. The 66-mm-long STK was composed of 10-mesh stainless steel screens with a wire diameter of 0.71 mm. It had a diameter of 156 mm. In the TWU, the 44-mm-long REG was made of stainless steel screens with a diameter of 83 mm. The screen had a mesh number of 60 and the wire diameter of 0.152 mm. The Ni–Cr resistance wires situated at the hot sides of the STK and REG were applied as the HHX in the prototype.

As shown in Figure 2, there are two TBTs in the system. The first one connected between the two stages was made from a standard stainless steel reducer from 6 to 3 inches.

The second TBT connected between the TWU and 2nd AHX was made from a standard 3-inch stainless steel pipe. Since the system was designed to operate with air at atmospheric pressure, the main resonators and cavities can be made of a standard 3-inch and 6-inch PVC pipes, respectively, instead of metal pipes in order to reduce construction costs considerably. The heating wires in HHXs were powered by two AC transformers separately that could regulate the voltage in the range of 0–240 V. The construction details of the CTE are shown in Table I.

In order to measure the hybrid operating mode and the distribution of the acoustic field along the system, nine piezoelectric pressure sensors (PCB PIEZOTRONICS model 113B28, measurement error $\leq 1\%$ FS), labelled P1–P9, were mounted as presented in Figure 2. Sensors P1–P4 were located along the up-resonator in front of the SWU, while sensors P5–P9 were attached along the down-resonator behind the TWU. The type-K thermocouples (with $\pm 1^\circ\text{C}$ accuracy), labelled T, were installed along the thermoacoustic cores to monitor the distribution of gas temperature; four probes were installed in the SWU, and another six probes were mounted in the TWU, as shown in Figure 2. All the dynamic signals of the pressure sensors and thermocouples were recorded by a high-speed data acquisition system.

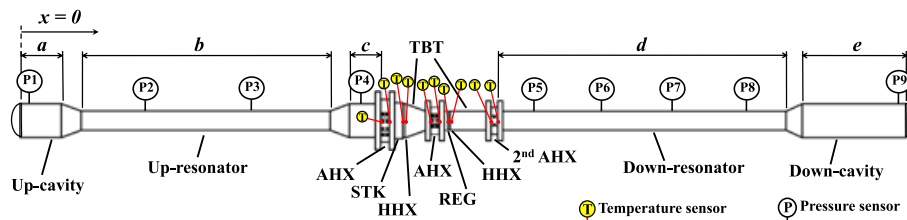


Figure 2. Cascade thermoacoustic engine as-built with measurement setup.

Table I. Construction details of the cascade thermoacoustic engine.

Parts name	Design features	Diameter (mm)	Length (cm)	Porosity	Mesh (wires/inch)	Wire dia (μm)
Up-cavity	6-inch PVC pipe	150	25			
Up-resonator	3-inch PVC pipe	81	107			
Up-resonator	6-inch PVC pipe	150	38			
<i>Standing-wave unit</i>						
AHX	Aluminium cross-flow HX	156	4	34%		
STK	Stainless steel mesh screens	156	6.6	78%	10	710
HHX	Coiled heating wire	156	1	85%		
TBT	Stainless reducer 6–3 inch	156–83	15			
<i>Travelling-wave unit</i>						
AHX	Water-cooled cross-flow HX	83	4	24%		
REG	Stainless steel mesh screens	83	4.4	72%	60	152
HHX	Coiled heating wire	83	1	80%		
TBT	3-inch stainless pipe	83	20			
2nd AHX	Aluminium cross-flow HX	83	3	35%		
Down-resonator	3-inch PVC pipe	81	160			
Down-cavity	6-inch PVC pipe	150	69			

4. PHASE-ADJUSTMENT METHOD

In the double Helmholtz resonator, a symmetry acoustic resonator has two cavities, each of volume V , at both ends. The resonator connecting both cavities has length Δl and cross-sectional area A . Based on acoustic network analysis, the resonance frequency of the double Helmholtz resonator is given by [13]

$$\omega = 2\pi f = a\sqrt{\frac{2A}{V\Delta l}} \quad (9)$$

where $a = \sqrt{\gamma p_m / \rho_m}$ is speed of sound. Basically, the double Helmholtz resonator is analogous to the CTE without thermoacoustic cores. However, the lossy thermoacoustic system is actually more complicated than the Helmholtz resonator in which the acoustic field requires the continuity, momentum and energy equations as shown in Eqs. (1–3) to be fully described. Notwithstanding, such a simple formula should be considered along with the computer simulation to find the effective solutions for phase adjustment of the REG in the TWU.

While thermoacoustic units are not inserted in the double Helmholtz resonator, the sweet spot should be located at the centre of the connecting tube. An asymmetry of acoustic impedance occurs unavoidably since the thermoacoustic units are introduced into the system. This causes an excursion of the sweet spot position in the CTE. Theoretically, the TWU can perform efficiently within high impedance and travelling wave phasing region where the phase difference between pressure and velocity of the REG is nearly zero. Thus, the effective solution is to prolong such sweet spot zone by reducing the resonance frequency of system. This also benefits to the starting-up of the acoustic oscillation because of decreasing the acoustic dissipation.

Referring to Eq. (9), increasing V , Δl or decreasing A , a would reduce the resonance frequency. These should be the feasible techniques for tuning the phase in the REG to improve the thermo-to-acoustic conversion. First, a simple method is to increase the volume of cavities, which is accomplished by increasing the length of the cavities. In the event that the end-cavities introduced are asymmetrical, the sweet spot is likely to move towards the larger cavity. Second, increasing the length of resonator also reduces the resonance frequency. The third technique is to decrease the cross-sectional area of resonator, which is performed by reducing the diameter of the resonator as well as inserting a pencil into the resonator, as described in [6]. Another scheme is to decrease the sound of speed by reducing the temperature of working fluid in the whole system. However, this technique seems to be difficult to implement.

Those proposed methods were applied to tune φ_z within the REG, except the scheme of changing the working fluid temperature. In order to investigate the effect of phase tuning, only the geometric dimensions of the down-cavity

and down-resonator were adjusted. These modifications were simulated, and some were also confirmed by experiments. The experimental details and results of the modifications of the CTE are presented in Table II. The abbreviations $a-e$ are the geometrical dimensions of the CTE as shown in Figure 2.

5. RESULTS AND DISCUSSION

In Table II, these phase-tuning experiments were performed. The heating powers supplied to the SWU and TWU were kept constant at 940 ± 10 W and 180 ± 2 W, respectively, in order to maintain the surface temperatures of the heating wire at 850 K. Once the thermoacoustic oscillation was detected, the onset temperatures (T_{os}) of both units were recorded. Since the oscillation was developed to steady state, the resonance frequency, pressure amplitude and hot-end temperatures of the system were examined to understand the responsiveness of phase-tuning process. According to Eqs. (5) and (8), the performance of the cascade engine here is monitored by the pressure amplitude at P9.

5.1. Effect of down-cavity length

In configurations 1–4, the length of the down-cavity (e) is shortened continuously, resulting in higher resonance frequency measured in experiments. As a result, the sweet spot zone ($-45^\circ \leq \varphi_z \leq +45^\circ$) in the REG should be wider with the volume of the down-cavity, as confirmed by the simulated results as provided in Figure 3. As seen, the sweet spot zone in the REG slightly increases with larger cavity, evidenced by the slopes of graph. Additionally, the sweet spot is shifted towards the hot-end of the REG, as the down-cavity becomes longer.

Figure 4 presents the distribution of the local impedance, which is the ratio of pressure and velocity, along the REG. The peak of impedance is located near the sweet spot, and also increases with smaller cavity. Theoretically, high impedance and travelling wave phasing are required in the REG. Thus, referring to Figures 3 and 4, configuration 1 offers a better travelling wave phasing, but configuration 4 provides a higher impedance. Therefore, the optimal length of down-cavity should be somewhere between them. This optimal value can be determined by analysing the distribution of pressure amplitude as shown in Figure 5. It can be observed that the pressure amplitude increases as the length of down-cavity becomes longer and reaches a peak at the certain length, after which it starts to decrease. This is because of the opposing effects of travelling wave phasing and high impedance as discussed above. So the optimal value found is about $e = 0.8$ m.

In Table I, since the length of down-cavity becomes shorter, the onset temperatures measured in both SWU and TWU decrease and then reach a minimum before climbing up. The lowest $T_{on, TWU}$ found in configuration 3 might be attributed to the effect of the position of sweet

Table II. Details of phase-adjustment experiments and their results.

Configurations of the modified system							Experimental results						
No.	a (cm)	b (cm)	c (cm)	d (cm)	e (cm)	Length (cm)	Impedance added into the down-resonator	$T_{on, SWU}$ (°C)	$T_{on, TWU}$ (°C)	$T_{H, SWU}$ (°C)	$T_{H, TWU}$ (°C)	$ P $ (kPa)	f (Hz)
1					205	615.5	No	453.3	476.9	465.9	528.1	4.19	55.9
2				160	110	520.5	No	371.2	399.6	417.1	492.0	10.10	56.5
3*	25	107	38		69	479.5	No	383.4	323.4	414.0	522.1	10.36	56.88
4				184	45.5	456.0	No	441.4	432.3	467.0	559.0	9.37	57.14
5				150	110	544.5	No	301.9	325.1	322.8	343.4	5.18	56.0
6						469.5	No	425.6	443.2	475.5	537.6	8.76	56.67
7							Pencil 1"-2 m long	301.2	311.6	352.8	414.9	10.22	57.17
8							Pencil 1.5"-2 m long	296.7	302.1	331.6	367.5	10.17	56.9
9	25	107	38	160	69	479.5	Pencil 2"-2 m long	289.0	294.2	312.5	325.8	9.97	56.64
10							#25 Mesh x 31-1 piece	381.5	320.7	415.0	513.5	8.90	56.85
11							#25 Mesh x 31-2 pieces	384.2	317.8	419.3	512.2	7.78	56.82
12							#25 Mesh x 31-3 pieces	419.7	330.5	432.8	526.7	6.25	56.63

Note: No. 3* is the optimal configuration.

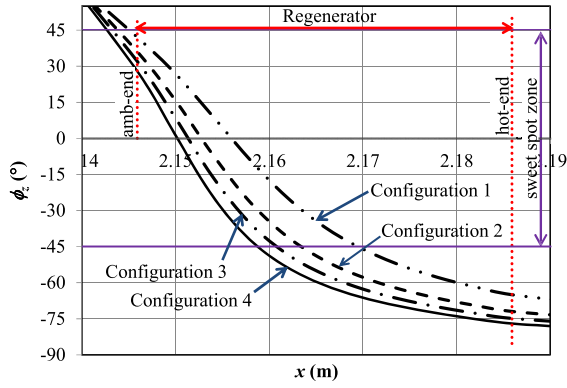


Figure 3. Effect of the length of down-cavity on the simulated phase of impedance within REG.

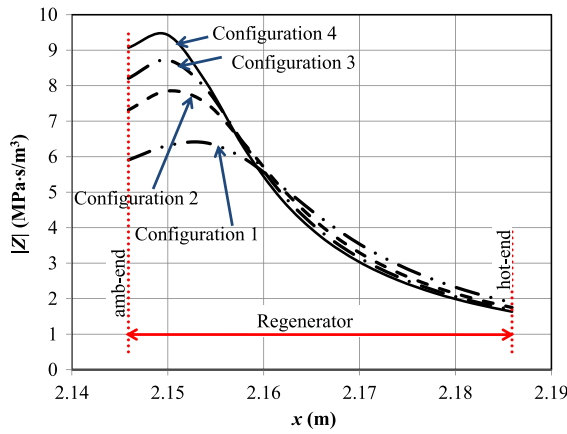


Figure 4. Effect of the length of down-cavity on the simulated impedance within REG.

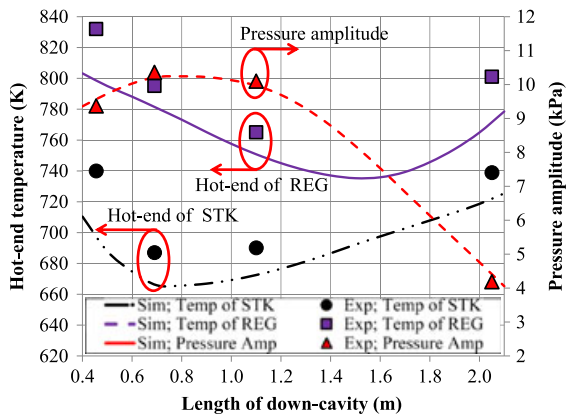


Figure 5. Effect of the length of down-cavity on the hot-end temperatures and the pressure amplitude.

spot and acoustic impedance as described in Figures 3 and 4. Meanwhile, configuration 2 offers the lowest $T_{on,SWU}$. Theoretically, $T_{on,SWU}$ is proportional to the local impedance, as referred to Eq. (6). As can be seen from Figure 6,

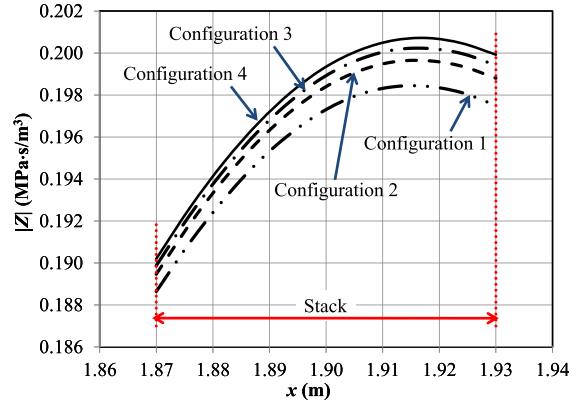


Figure 6. Effect of the length of down-cavity on the simulated impedance within STK.

the magnitude of impedance within the STK increases with smaller cavity. When the down-cavity becomes shorter, a higher temperature of the SWU is required to self-oscillate. However, the longer cavity also causes a larger viscous loss, resulting in the increase of T_{on} of both the SWU and TWU.

Furthermore, Figure 5 also shows that the variations of steady-state temperature of the STK and REG correspond to that of T_{on} as discussed above. There are the lowest hot-end temperatures of the STK and REG at about $e=0.8$ m and $e=1.5$ m, respectively. As clearly seen, the TWU requires a higher temperature than the SWU needed to produce acoustic wave. This is because of the much smaller hydraulic radius of the REG comparing to the STK.

The comparison between the experimental and simulation results is also demonstrated in Figure 5. It can be seen that the predicted results can capture well the trend of the measured temperatures and pressure amplitude. However, the measured hot-end temperatures of the STK and REG are slightly higher than the prediction. This is because of no heat loss taken into account in the simulation. It considers only the heat involved in the thermoacoustic effect.

5.2. Effect of down-resonator length

When the length of down-resonator (d) becomes longer as shown in configurations 2, 5 and 6, the measured resonance frequency decreases. Figure 7 presents the effect of the length of the down-resonator on the impedance phase and the frequency. As seen, the simulation also agrees that the frequency decreases linearly with the increase of down-resonator length. ϕ_z at both hot-end and ambient-end of the REG increases. This result implies that the sweet spot shifts rightward from the ambient-end to the hot-end of the REG. Therefore, the thermo-to-acoustic conversion of the REG gradually increases because of travelling wave phasing, as the down-resonator becomes longer. Consequently, the longer down-resonator can reduce the onset

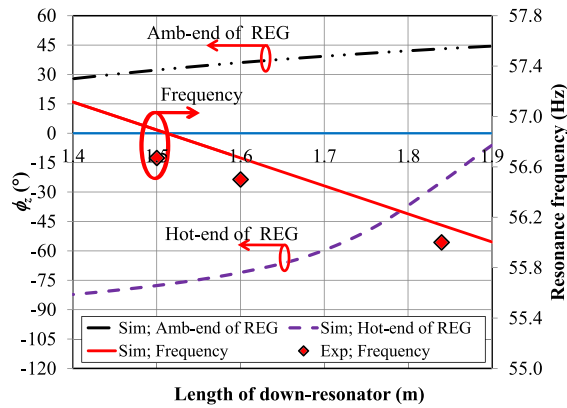


Figure 7. Effect of the length of down-resonator on the impedance phase and the frequency.

and steady-state temperatures of the system as illustrated in Figure 8.

However, unlike the effect of down-cavity, there is no increment of the hot-end temperatures observed in the case of longer resonator. This can be explained that the increased ϕ_z is still close to zero, so that the high energy conversion can be kept. Furthermore, the surface area increased because of longer resonator is much less than that of cavity, and this circumstance leads to lower viscous loss. The variation of pressure amplitude as shown in Figure 8 is also similar to that the case of down-cavity. However, it is worth noting that the acoustic field is more sensitive to the effect of down-resonator than that of the down-cavity. This is because the down-resonator has a stronger effect on the resonance frequency compared with the down-cavity case.

In Figure 8, the discrepancy between the measured and simulated temperatures becomes smaller, as the down-resonator is longer. This might be that the heat loss reduces with the surface temperature of thermoacoustic core.

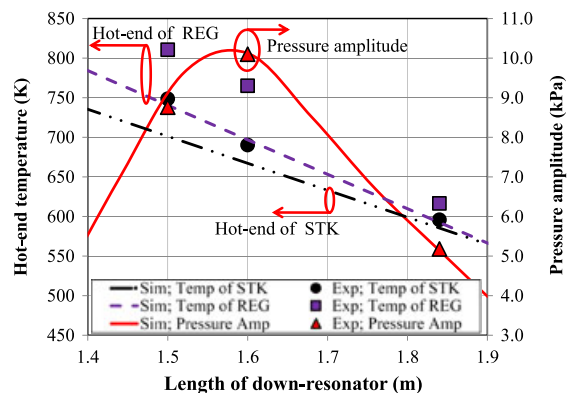


Figure 8. Effect of the length of down-resonator on the simulated hot-end temperatures and the pressure amplitude.

5.3. Effect of inertance impedance

In configurations 7–9, a 2-m-long PVC pipe with different diameters used as a pencil was inserted into the down-resonator section in order to increase the inertance impedance. The insertion of the pencil not only reduces the cross-sectional area, but also increases the surface area. The extra dissipation of acoustic power arises because of increasing both the surface area and the velocity therein.

Figures 9 and 10 provide the simulation and experimental results that indicate how the ratio of pencil to the total areas affected the acoustic field of system. As seen, the effect of the pencil ratio on the acoustic field is generally similar to that of the down-resonator. That is, as the diameter of pencil becomes larger, the frequency of system decreases. This allows the sweet spot to shift rightwards. Consequently, the hot-end temperatures of the STK and REG decrease with the ratio of pencil area. There is a peak of pressure amplitude located at the pencil ratio of about 10%. When the diameter of pencil becomes overlarge, the pressure amplitude drops considerably. This is because of tremendous velocity, leading to enormous viscous

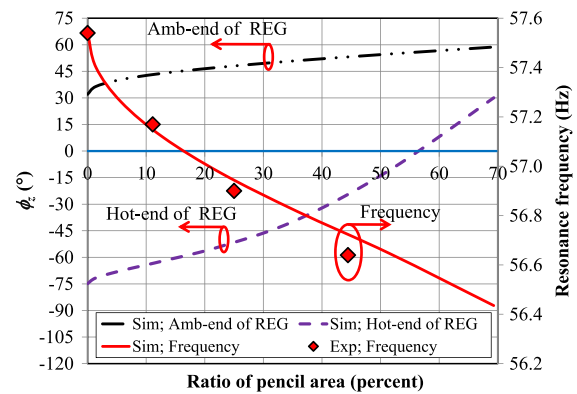


Figure 9. Effect of pencil insertion on the impedance phase and the frequency.

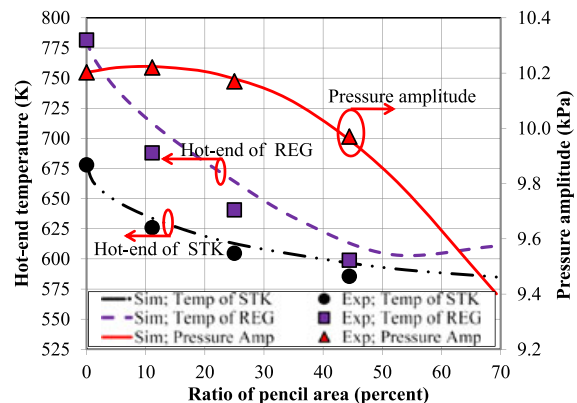


Figure 10. Effect of pencil insertion on the hot-end temperatures and the pressure amplitude.

dissipation. Moreover, the simulated and experimental results are in good agreement.

Nevertheless, the pencil ratio has less effect on frequency compared with the effect of down-resonator length. This is because the frequency is mainly proportional to the total length of system. In addition, the reduction of hot-end temperatures of the STK and REG is less than that the case of down-resonator length. The explanation is that there is a huge reduction of resonance frequency in case of down-resonator length, in which the temperature gradient, as illustrated in Eq. (3), depends on the frequency of system ($\omega = 2\pi f$). Again, in the range of high pencil ratio, the increase of hot-end temperature of the REG is observed. It can be explained that the energy conversion of the REG becomes lower, so that the heat converted into acoustic power reduces, resulting in the accumulation of temperature. Interestingly, the reduction of pressure amplitude in this event is small, compared with the cases of down-resonator and down-cavity.

Even though this method can significantly reduce the temperatures of the system, the decrease of gas temperature in the system also reduces the pressure amplitude as well. In such a circumstance, the extra viscous loss and reduced pressure amplitude should be taken into account. Accordingly, the optimal cross-sectional area of pencil is about 10% of the total area, which is also consistent with the experimental results of Gardner and Swift [6].

5.4. Effect of resistance impedance

The stainless steel mesh screens were installed at the down-resonator with $x = 4.04$ m, in order to observe the effect of resistance impedance on the acoustic field in the system. The simulated results are presented in Figures 11 and 12. Moreover, as seen in Table II of configurations 3 and 10–12, increasing the resistance by adding a number of mesh screens reduces the resonance frequency of the system. This is because the resistance reduces the volumetric velocity in the system. According to the continuity equation (cf. Eq. (1)), the decrease of velocity causes the

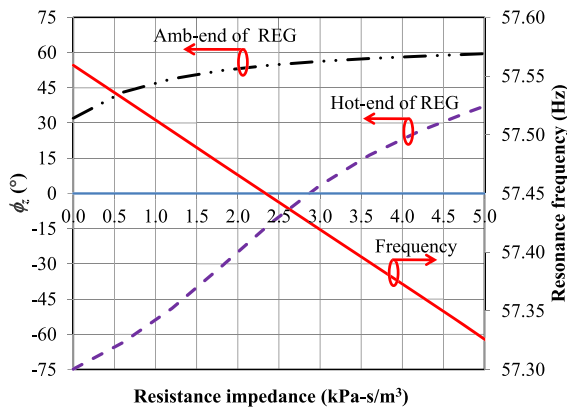


Figure 11. Effect of resistance impedance on the simulated impedance phase and the frequency.

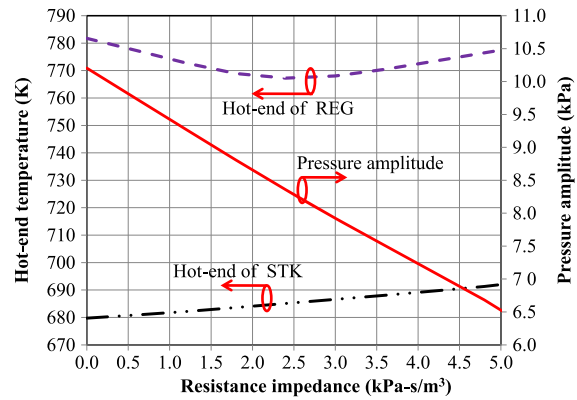


Figure 12. Effect of resistance impedance on the simulated hot-end temperatures and the pressure amplitude.

reduction of pressure amplitude as shown in Figure 12. These reductions of both pressure and velocity occurred in the right portion of system, where the resistance is mounted, are larger than that in the left portion of system. Subsequently, the sweet spot is necessary to move rightwards away from the REG, as the resistance increases, to maintain the balance of the acoustic impedance in the system. This finding is also testified by the numerical results, as shown in Figure 11. Unfortunately, the exact resistance impedance of mesh screen cannot be measured here.

The temperature of the REG, as displayed in Figure 12, decreases as the resistance impedance increases and reaches a minimum point, after that it starts to increase. The reason can be explained in the same manner as the effect of down-cavity. As ϕ_z at the hot-end of the REG becomes closer to zero, the T_H of the REG is lower, owing to higher energy conversion. However, unlike any other effects, the STK requires a higher temperature, as the resistance becomes larger. This can be explained by referring to Eq. (5), in which the acoustic power generated in the SWU mainly depends on the gradient temperature across the STK. Since the resistance is increased in the system, the more acoustic power produced by the STK is needed in order to balance such a dissipated acoustic power. Consequently, the hot-end temperature of the STK steadily increases with the resistance impedance.

6. CONCLUSIONS AND FUTURE WORKS

This project was undertaken to improve the performance of the CTE, consisting of one SWU and one TWU connected in series. The travelling wave phasing and high impedance within the REG are required to achieve high efficiency. The phase-adjustment techniques were investigated numerically and experimentally by increasing the volume of cavity, increasing the length of resonator, decreasing the cross-sectional area of resonator and adding the resistance impedance into the resonator. The numerical and experimental results show that all the proposed

schemes can shift the position of the sweet spot within the REG. When the sweet spot is close to the hot-end of the regenerator, the energy conversion becomes excellent, resulting in the decrease of the temperatures required for self-oscillation. Here, to achieve both low onset temperature and high pressure amplitude, the potential method for adjusting the sweet spot is to reduce the flow area of down-resonator by inserting the appropriate pencil. Furthermore, the length of down-resonator is relatively sensitive to the acoustic field in the system; therefore, this should be taken into careful consideration. Additionally, the simulated results can capture well the trend of the measured temperatures, pressure amplitude and frequency. The next step of research is to integrate the cooler unit into the CTE, which would be considered as sustainable refrigeration system if heat source of the CTE is waste heat or renewable energy.

ACKNOWLEDGEMENTS

The authors would like to gratefully acknowledge the financial support provided by Thammasat University and the Thailand Research Fund (TRF) under the Contract No. TRG5780168.

REFERENCES

- Jaworski AJ, Mao X. Development of thermoacoustic devices for power generation and refrigeration. *Proceedings of the Institution of Mechanical Engineers, Part A: Journal of Power and Energy* 2013; **227**:762–782.
- Ceperley PH. A pistonless Stirling engine—the traveling wave heat engine. *Journal of the Acoustical Society of America* 1979; **66**:1508–1513.
- Ceperley PH. Gain and efficiency of a short traveling wave heat engine. *Journal of the Acoustical Society of America* 1985; **77**:1239–1244.
- Yazaki T, Iwata A, Maekawa T, Tominaga A. Traveling wave thermoacoustic engine in a looped tube. *Physical Review Letters* 1998; **81**:3128–3131.
- Backhaus SN, Swift GW. A thermoacoustic-Stirling heat engine: detailed study. *Journal of the Acoustical Society of America* 2000; **107**:3148–3166.
- Gardner DL, Swift GW. A cascade thermoacoustic engine. *The Journal of the Acoustical Society of America* 2003; **114**:1905–1919.
- Luo E, Dai E, Ling H. Chapter 73—Basic operation principle of a novel cascade thermoacoustic prime mover. In *Proceedings of the Twentieth International Cryogenic Engineering Conference (ICEC20)*. Elsevier Science: Oxford, 2005; 317–320.
- Ling H, Luo E, Dai W, Li X. Chapter 77—Numerical simulation on a novel cascade thermoacoustic prime mover. In *Proceedings of the Twentieth International Cryogenic Engineering Conference (ICEC20)*. Elsevier Science: Oxford, 2005; 333–336.
- Hu Z, Li Q, Xie X, Zhou G, Li Q. Design and experiment on a mini cascade thermoacoustic engine. *Ultrasonics* 2006; **44** Supplement:e1515–e1517.
- Hu ZJ, Li Q, Li Q, Li ZY. A high frequency cascade thermoacoustic engine. *Cryogenics* 2006; **46**:771–777.
- Biwa T, Tashiro Y, Mizutani U, Kozuka M, Yazaki T. Experimental demonstration of thermoacoustic energy conversion in a resonator. *Physical Review E* 2004; **69**:066304.
- Ward B, Clark J, Swift GW. *Design Environment for Low-Amplitude ThermoAcoustic Energy Conversion (DELTAEC) programme*. Los Alamos National Laboratory: New Mexico, USA, 2008. Version 6.2 b3.
- Swift GW. *Thermoacoustics: a unifying perspective for some engines and refrigerators*. Melville, NY: Acoustical Society of America through the American Institute of Physics, 2002.